

LA-UR-10-2380

Approved for public release;
distribution is unlimited.

Title: Critical Comparison of Two Independent Measurements of Residual Stress In An Electron-Beam Welded Uranium Cylinder: Neutron Diffraction and the Contour Method

Author(s): D.W. Brown
T.M. Holden
B. Clausen
M. B. Prime
T.A. Sisneros
H. Swenson
J. Vaja

Details: Acta Materialia, ~~ACTA~~ **59**(3), pp. 864-873.
doi:10.1016/j.actamat.2010.09.022



Los Alamos National Laboratory, an affirmative action/equal opportunity employer, is operated by the Los Alamos National Security, LLC for the National Nuclear Security Administration of the U.S. Department of Energy under contract DE-AC52-06NA25396. By acceptance of this article, the publisher recognizes that the U.S. Government retains a nonexclusive, royalty-free license to publish or reproduce the published form of this contribution, or to allow others to do so, for U.S. Government purposes. Los Alamos National Laboratory requests that the publisher identify this article as work performed under the auspices of the U.S. Department of Energy. Los Alamos National Laboratory strongly supports academic freedom and a researcher's right to publish; as an institution, however, the Laboratory does not endorse the viewpoint of a publication or guarantee its technical correctness.

Critical Comparison of Two Independent Measurements of Residual Stress In An Electron-Beam Welded Uranium Cylinder: Neutron Diffraction and the Contour Method

D.W. Brown¹, T.M. Holden², B. Clausen¹, M. B. Prime¹, T.A. Sisneros¹, H. Swenson¹, J. Vaja³

¹Los Alamos National Laboratory, Los Alamos, New Mexico 87545, USA

²Northern Stress Technologies, Deep River, Ontario, Canada K0J 1P0

³Atomic Weapons Establishment, Aldermaston, Reading, Berkshire, RG7 4PR UK

Abstract

Neutron diffraction and contour method measurements were conducted to assess the stresses associated with an electron-beam, circumferential, partial penetration weld of a uranium tube. To obtain reasonable results in the coarse-grained base metal, the specimen was continuously rotated during the neutron experiments to average over the entire circumference. The severe anisotropic character of uranium, which has an orthorhombic crystal structure, forces a number of judicious choices to be made in the neutron analysis. For the contour method, the cylindrical geometry necessitated the development of a two step process, and discontinuities across the unwelded portion of the joint required special treatment. High tensile hoop stresses (~300 MPa) were found in the center of the weld close to the outside diameter. Balancing hoop compression was observed in the far-field stress profile. Also, a tensile axial stress (85 ± 25 MPa) was observed near the outer diameter.

Keywords : Uranium, Residual Stress, Neutron Diffraction, Anistropy

1. Introduction

Residual stresses are often critical to the structural integrity of manufactured components because they can accelerate or retard many failure processes [1]. Residual stresses are particularly important in fusion welds because of high, typically tensile, stress magnitudes combined with often unfavorable microstructure changes near the weld. Residual stress measurement, once a challenge, has become almost routine for certain components, welded plates for instance, made from cubic metals such as steel or aluminum [2]. However, residual stress measurements in other materials, notably lower symmetry metals such as Zircaloy-2 [3] and beryllium [4] as well as complicated geometrical components still provide a significant challenge. In such cases, the use of at least two independent measurements is prudent in order to provide confidence in the accuracy of the results. This work uses two techniques, with dissimilar assumptions to measure the residual stresses in a particularly challenging part, specifically, a welded as-cast uranium cylinder.

Diffraction techniques are typically well-suited to the determination of the macroscopic stresses associated with welds since the spatial resolution available (of order mm) is generally less than the spatial extent of the region of high stress and the accuracy of the method is adequate. In particular, neutron diffraction is a viable technique to measure stresses in uranium because it readily allows penetration of the neutron beam through several centimeters of material. For a complete review of the method see ref. [5].

However, because of its orthorhombic crystal structure, uranium represents a difficult material on which to measure residual stresses with diffraction techniques.

Neutron diffraction measurement of stress is complicated, particularly in low symmetry metals, because of the presence of type II, or intergranular stresses which arise due to elastic, thermal, and plastic anisotropy, and superimpose on the type I macroscopic stress field which is usually the target of the measurement. The low crystal symmetry of uranium results in anisotropic elastic and plastic mechanical response [6] as well as anisotropic coefficients of thermal expansion in the crystal coordinates. This is evident in the uranium single crystal elastic stiffness matrix [7] given in Table 1. Despite the complexity, a handful of publications on residual stresses in uranium measured by diffraction techniques may be found in the literature [8-11].

Mechanical relaxation measurements of residual stresses make excellent independent validations of diffraction measurements because they rely on entirely different assumptions and are much less sensitive to the type II stresses that cause difficulties for diffraction methods. For this application, the contour method was chosen for its ability, virtually unique among relaxation methods, to measure a cross-sectional stress map with only a single cut [12-16]. The technique has been successfully validated and applied on many weld specimens [17-23].

2. Experimental Description

2.1 Sample Figure 1 shows a schematic, drawn approximately to scale, of the welded uranium sample characterized in this work. The individual cylinders were as-cast uranium with a high carbon content of roughly 700 ppm by weight. The sample had the form of a tube 131 mm in axial length with an inner diameter (ID) of 122 mm. At one end, termed the “A” end the outer diameter (OD) was 149 mm but at the opposite end,

the ‘B’ end, the outside surface was chamfered down to an OD of 137 mm, resulting in a wall thickness of 14 mm at the ‘A’ end and 8 mm at the ‘B’ end.

The cast cylinders were machine fit at a step joint, as shown schematically in fig. 1. The weld was a two-pass partial-penetration, autogenous electron beam weld centered at 64.8mm from the ‘A’ end. The first pass, with the e^- beam focused, penetrated roughly half of the thickness, bonding the two cast cylinders. The e^- beam was then defocused for the second, cosmetic weld pass. Figure 2 shows a macrograph of the base metal, heat affected zone, and weld pool. While it is difficult to distinguish grains in figure 2, single grains with dimension of 2 mm or larger are apparent in the as-cast microstructure of the base metal. The melt areas of both passes are clearly visible in the macrograph and are also shown schematically in fig. 1. The microstructure is upset in the weld and heat affected zone (HAZ) causing a much finer grain structure in the melt region and a weakening of the crystallographic texture in the melt region and HAZ. Uranium carbides are much finer and equally distributed in the fusion zone compared to both the HAZ and as-cast structure suggesting that they had been dissolved in the melt and re-precipitated on cooling.

2.2 Neutron Diffraction Measurement of Stress The neutron diffraction measurements were completed on the SMARTS diffractometer at the Lujan Center at the Los Alamos Neutron Science Center (LANSCE), Los Alamos National Laboratory. Where possible, the experimental procedure followed the standard test method for determining residual stresses by neutron diffraction [24]. Details of SMARTS have been published elsewhere [25], and only a brief description will be given here.

SMARTS is a time-of-flight (TOF) diffractometer, with a continuous incident energy spectrum peaked at $\sim 1.5\text{\AA}$, but usable at wavelengths from 0.7\AA to 5.5\AA . The cross section of the incident beam was defined by boron nitride apertures which were 3mm wide and 12mm high for the measurement of the radial and axial strains where the height of the slit has minimal influence on the along-wall resolution. The vertical slit was restricted to 3mm close to the weld in the hoop and radial configuration where the height affects the along-wall resolution and to 6mm high well away from the weld where the strain gradients are small.

Two detector panels are located at $\pm 90^\circ$ from the incident beam and span $\pm 15^\circ$ in the vertical and horizontal planes. Because the incident neutron beam has a continuous energy spectrum, each detector panel records an entire diffraction pattern (d-spaces from 0.5 to 4\AA) simultaneously and with parallel diffraction vectors bisecting the incident and diffracted beam vectors, i.e. at $\pm 45^\circ$ from the incident beam. Each detector is focused by a radial collimator to accept neutrons from a 3 mm section along the direction of the beam. The crossover of the incident beam and field of view of the radial collimators defines a “gauge” volume from which the diffraction data is collected and over which average lattice parameters are determined. The size of the gauge volume relative to the sample dimensions is roughly indicated in Figures 1 and 2.

The sample was positioned optically with an accuracy of $\pm 0.1\text{mm}$ with the aid of two computerized LeicaTM theodolites. The sample position was verified by “wall scans” of the surface through the gauge volume. The sample was mounted on a sturdy fixture which could be rotated about a horizontal axis (manually) to bring the cylinder axis of the sample either vertical or horizontal. When the sample axis was horizontal the two banks

recorded the axial (+90° bank) and radial (-90° bank) strains and when it was vertical the two banks recorded the radial (+90° bank) and hoop (-90° bank) strains. The measurements of the radial strains were repeated in the two configurations (in different detector banks) and agreed to within uncertainty.

The sample was swept through the gauge volume by a motorized translator table and the lattice parameters were mapped as a function of position. The neutron diffraction collection times were 20 to 30 minutes per point, depending on the gauge volume used. Measurements were made on several through-thickness loci (2.8, 4.9, 7.0, 9.1, and 11.2 mm from the ID) along the entire length of the tube so as to be able to check the stress balance across the sample.

Initial attempts to measure the residual stress [26] in the welded uranium cylinder resulted in very scattered data because of the large grain size of the as-cast microstructure relative to the gauge volume [5]. Thus, in the current measurements, the tube was rotated continuously on its own axis at a rate of one revolution per minute increasing the number of grains sampled by the neutron beam by a factor of about $2 \times \pi \times 70/3$, or 140 times, and removing this source of scatter and hence uncertainty. This comes at the expense of averaging the residual stresses around the cylinder. While rotating, the OD of the cylinder was monitored with a dial indicator and found to be “round” to within ± 0.4 mm, which is small relative to the gauge volume.

2.3 Diffraction Data Analysis Each diffraction pattern was analyzed by Rietveld refinement using the General Structural Analysis Software (GSAS) [27] developed at LANSCE. Pertinent to this study, the three lattice parameters, a, b, and c were determined

by the refinement as well as the pole density of many hkl's in the diffraction pattern along the specific sample directions.

2.3.a Residual Strain Determination The residual strains are calculated from the fractional difference of the spatially varying lattice parameters relative to appropriate reference lattice parameters, a_{ref} , b_{ref} and c_{ref} , for example

$$\epsilon_a = (a - a_{ref}) / a_{ref}. \quad (1)$$

Because there was no companion weld from which reference coupons could be removed, reference lattice parameter measurements could not be completed at the time of the residual stress measurement in the as-welded sample as would be the preferred procedure [5, 24]. Rather, reference specimens were cut from the base and weld metals subsequent to the dissection necessary for the contour measurements.

Once again, the large grain size complicated the determination of the reference lattice parameters. Following the longitudinal cuts made for the contour measurement, two roughly 65° arcs, each 3.75 mm thick, were cut (electric discharge machined or EDM'd) transverse to the axis of the welded tube from the base metal and weld metal. Subsequently, a series of thin partial penetration radial cuts at 3.75 mm intervals were made from the OD toward the ID to within 3mm of the ID, effectively relieving the axial and hoop components of the residual strain. Analogous to the measurement of the lattice parameters in the intact part, diffraction data were collected as the arc was slowly rotated from one end to the other over the duration of the measurement. In this manner, good quality diffraction patterns were obtained from stress relieved samples removed entirely from the base metal and weld metal.

Due to the logistical difficulties in transporting and machining uranium, several months passed between the measurement of the whole sample and the reference sample, during which the instrument was reconfigured several times. **Because of this, the lattice parameters measured in the references do not match, in an absolute sense, those measured in the uncut sample, to within the accuracy of the relative strains determined within a single setting.** The result of this is that the reference specimen has been used to verify that the reference lattice parameters are the same within uncertainty in the base metal and weld pool, that is there are no chemical strains present, but they cannot be used as an absolute reference. Rather, we have used lattice parameters determined at the edge of the cylinder where the macroscopic residual stress is expected to be small as reference. Force balance calculations and consideration of boundary conditions, **e.g. the axial and radial stress are zero far from the weld**, were used to validate the choice of reference lattice spacing.

To determine a representative macroscopic strain field from the observed lattice strains, the three lattice strains were averaged with weighting based on their measured textural strength along each sample direction, e.g.

$$\varepsilon_{macro} = \sum_{i=a,b,c} w_i \varepsilon_i . \quad (2.)$$

This method accounts for the texture evolution from the base metal to the weldment and corresponds to that outlined by Daymond [28] for determining representative residual strains from anisotropic crystals, except we utilize the lattice parameters (a,b, and c) obtained from Rietveld refinement instead of multiple single peaks (hkl) because of practical intensity considerations.

Given the texture of the as-cast material (shown later) and the single crystal stiffness tensor [7], an effective polycrystalline stiffness tensor was calculated using an elastic-plastic self-consistent (EPSC) model [29, 30]. The resulting stiffness tensor, shown in Table 1, is relatively isotropic compared to the measurement uncertainties. Thus, for simplification, an isotropic stiffness tensor, also shown in table 1 was adopted for the stress calculation at each measurement position.

2.3.b Crystallographic Texture Using the time-of-flight technique with fixed detector position, the diffraction vectors of every hkl recorded in the individual detector banks are parallel. Thus, the individual peak intensities, corrected for structure factor, absorption, etc, may be mapped directly onto an irreducible stereograph (quadrant for orthorhombic uranium) to form an inverse pole figure (IPF). Moreover, because the intensities are determined by the Rietveld refinement, significant peak overlap may be accepted and many crystal orientations (hkl) even at relatively small d-spaces may be mapped onto the IPF resulting in confidence in drawing contours. A single inverse pole figure can be determined from each diffraction pattern e.g. along the hoop, radial or axial directions of the sample. Historically, this procedure has produced IPF's which closely match those calculated from complete orientation distribution functions [31].

2.4 Contour Method Determination of Residual Stress A novel, two-step variation of the contour method was used to measure hoop stresses over a radial-axial cross-section of the cylinder. Because hoop stresses can have a bending moment through the thickness of a cylinder (it is balanced on the opposite thickness), cutting radially into the cylinder can cause high loads at the cut tip and result in yielding and other difficulties [32, 33]. It has been proposed [34] for contour and slitting (crack compliance) measurements to first

sever the cylinder, changing the cross section from an “o” to a “c.” How much the “c” springs open or closed is monitored to determine the bending moment released. Then a contour measurement is performed on the remaining portion of cylinder, now moment free. That procedure was implemented in this work.

A total of three EDM cuts were made on the uranium tube in the radial direction for the contour method. Each cut operation implemented “skim cut” settings with a 100 μm diameter brass wire to reduce the introduction of new stresses. Pairs of scribe lines, separated by about 6mm, were made along the length of the cylinder on the OD. The first EDM cut was made between the scribe lines with the wire oriented axially and translated radially. After unclamping, the relative displacements of the scribe lines were optically measured at 25 mm increments along the length of the tube. The second cut, taken at $\sim 120^\circ$ counter-clockwise from the first radial cut direction, was used to provide access for the third cut, but has no significant effect on the stresses measured by the third cut. The larger remaining section of the specimen was then used in the contour method. A stainless steel fixture was machined to securely clamp the part along the ID and OD surfaces. To achieve better cut quality, the wire was now oriented in the radial direction and translated axially to make the cut.

After the final cut, the contours of the opposing surfaces were measured in a temperature controlled environment using a Coordinate Measuring Machine (CMM) with a 0.5 mm diameter ruby touch probe. The surfaces were scanned on a 0.5 mm grid giving about 6800 points per surface.

2.5 Contour Method Data Analysis The determination of the stresses from the contour data assumed a homogeneous continuum in order to elastically calculate the

macroscopic (Type I) residual stresses. The heterogeneity from the large grains should not have a significant effect. The Type II residual microstresses and corresponding elastic residual strains are expected to vary significantly grain to grain and influence the neutron measurements. Such residual strains can vary discontinuously because they are eigenstrains, not total strains, and need not satisfy compatibility. The contour method measures total elastic deformations after stress is relieved by cutting. The grain to grain variations of these relaxation strains are constrained by compatibility, which reduces grain to grain variations. The measured contours did not show any evidence of features corresponding to individual grains.

The contour method analysis assumed isotropic elasticity as did the neutron analysis and with the same values. A separate analysis with the anisotropic effective polycrystalline stiffness tensor, EPSC in Table 1, changed the stresses by an insignificant 7 MPa or less everywhere.

A 3D elastic finite element (FE) model was used to calculate the stresses from the contour data. The perimeter of the cross-section was modeled based on the CMM data, and then the surface was meshed with 2D elements. The elements were not joined across the un-joined portion of the step joint. The 2D surface mesh was extruded circumferentially to produce 3D meshes 180 degrees and 120 degrees in extent to analyze the first and third cut data, respectively. The elements were approximately cubes 1.4 mm on a side near the cut surface and graded to be coarser in the circumferential direction farther away. The 180 degree mesh had almost 90,000 bi-quadratic (20 node) reduced integration hexahedral elements. No contact surfaces were used in the un-joined portion

of the joint. Observation of the joint after cutting, e.g. Figure 2, indicated that the gaps between the surfaces were sufficient to prevent contact.

The first FE analysis, using the 180 degree mesh, was used to calculate the bending moment stresses released in the first cut. A symmetry plane was used to constrain one surface and concentrated forces were used to apply a bending moment on the opposite surface. The force magnitude was scaled until the surface in the half-symmetry model closed to reverse the amount of opening observed experimentally.

Converting the raw data into a form suitable for stress calculation generally followed standard procedure [18, 33], except for some special care because of the discontinuity in the surface contours across the un-welded portion of the joint. The two opposing surfaces created by the cut were aligned with each other and then the data was interpolated onto a common grid and averaged. To handle the discontinuity, the surface was divided into two regions on either side of the weld joint with a few mm of overlap only in the part joined by the weld. Each region was then smoothed using quadratic bivariate spline fits with an optimal knot spacing determined to be about 5 mm. The two smooth surfaces were then joined together which resulted in discontinuities matching the data but a continuous joint in the weld region where the two regions overlapped. The joined surface was evaluated at nodal coordinates in order to apply displacement boundary conditions to the FE model and deform the cut surface into the opposite of the measured contour in the direction normal to the surface [12].

3. Results

3.1 Texture Variation Figure 3 shows inverse pole figures representing the preferred crystallographic orientation along the radial, hoop, and axial directions of the

sample measured near the ‘B’ end of the base metal and in the weld pool/HAZ. In the base metal, the radial sample direction (presumably the direction of heat flow during cooling from casting) is dominated by crystallites with (010) plane normals aligned with this direction. Relative to the strong preferred orientation in the radial directions, the axial and hoop sample directions are rather evenly comprised of crystallites with plane normals between the (100) and (001) plane normals. The preferred orientation in the weld pool/HAZ has a similar trend, but is significantly weaker in strength than in the base metal.

Figure 4 shows the evolution of the pole density in multiples of random distribution (MRD) of the primary crystal axes of the orthogonal structure along the radial direction moving from the base metal, through the HAZ and weld pool, and back to the base metal. Again, (010) plane normals are predominantly aligned with the sample radial direction outside of the welded area, but the texture weakens significantly (all values tend to unity) in the HAZ and weld pool.

3.2 Residual Strains

3.2.a Neutron Diffraction Figure 5 shows the measured residual strains averaged according to eq. (2) as a function of distance from the weld centerline and three different depths. The uncertainties shown are strictly statistical in nature and do not reflect any systematic uncertainties such as in the choosing of a reference lattice spacing. The measured reference lattice parameters in the base metal and weld metal were within uncertainty of each other. Thus, despite the microstructural evidence that the carbides have been re-distributed in and near the weld pool, no chemical strains were observed and the strains shown in figure 5 may be interpreted as mechanical in nature.

The largest residual strains are tensile hoop strains near the OD at the weld centerline. There is a strong through-thickness variation of the hoop strain near the weld. Near the inner diameter the hoop strains are compressive close to the weld line, but still manifest a local maximum at the centerline. Like the hoop strains, the axial strains vary considerably with depth. Near the OD, the axial residual strains are tensile and extend far from the weld. In the center of the through-thickness, the axial strains are positive far from the weld with a compressive spike of $\sim 4 \times 10^{-4}$ in the vicinity of the weld. Near the ID, the axial strains are mostly negative. The radial strains are within uncertainty of zero everywhere except within ± 10 mm of the weld centerline, where they are compressive, or zero in the case of the measurement near the ID.

3.2b Contour Method As a result of the first cut, the cylinder sprung open by 1.27 ± 0.01 mm uniformly along the length of the cut. The calculated bending moment stresses varied nearly linearly from about -60 MPa on the inner surface to about 50 MPa on the outer surface. These bending stresses were superimposed with those determined from the surface contour to calculate the residual stress field in the as-welded tube.

Figure 6 shows the contours measured by the CMM on the two surfaces created by the third cut. One of the surfaces has been flipped to match the orientation of the other. The peak-to-valley range of the contours exceeds 40 μ m. The close agreement between the two contours indicates that the part was clamped well during the cut and the experimental conditions were symmetric. The contours are low in the weld region (right side, mid height in this figure, see Figure 1) as would be expected if tensile stresses were relieved. A height discontinuity is evident cross the joint near the ID, which is

mechanically admissible because of the un-joined material associated with the partial penetration weld.

Figure 7 shows the FE model after the displacements were applied to the cut surface to calculate the stresses from the third cut. The displacements are magnified by a factor of 300. The discontinuity across the joint is evident in Figure 7. The stresses calculated in this analysis were added to the bending moment stresses released by the first cut to determine the total residual stress. A one standard deviation uncertainty of ± 25 MPa was estimated considering random errors in measured contours and uncertainty in the amount of data smoothing [18] but not any systematic errors.

4. Discussion

4.1 Residual Stress Profile The hoop, axial and radial components of the residual stress determined from neutron diffraction measurement of lattice strain are shown in figure 8. The uncertainty in the neutron stress measurements have been propagated from the statistical uncertainties in the measured strains, and are mostly between 35 MPa at the edges where the texture is strong, and 60 MPa at the center where the texture is more random. The peak tensile hoop stress at the weld center line near the OD is 260 MPa. This falls off quickly moving toward the ID and the stress 2.8mm from the ID is actually slightly compressive. The hoop stress also drops off quickly moving axially away from the weld centerline, is compressive roughly 20mm from the centerline, and approaches zero far from the weld. The axial stress is tensile near the OD and compressive near the ID, but extends much further along the axis than the hoop stresses. The radial stresses are everywhere within uncertainty of zero with the possible exception of two small negative excursions in the center thickness and on the edge of the HAZ at ± 5 mm from the

centerline. The near zero value of the radial residual stresses, especially in the far field, suggests that the reference lattice parameters were reasonable.

For quantitative comparison purposes, figure 9 shows the hoop component of the residual stress as a function of distance from the weld along the center of the thickness determined by both neutron diffraction and the contour method. In order to compare the neutron diffraction and contour results, the contour results were averaged over an area corresponding to that of the neutron gauge volume. The trends and peak to valley amplitudes of the measured data agree well, but the stresses measured by diffraction are systematically about 50 MPa below those measured by mechanical relaxation.

Within uncertainty, the bending moment stresses calculated from the spring open of the first cut match the through-thickness trends in the hoop stresses measured by neutron diffraction. This agreement validates the two-step process used for the contour method measurement.

For more of an overview, Figures 10a-d show contour plots of the hoop stresses measured by (a.) neutron diffraction (b.) mechanical relaxation and (c.) the axial stress measured by neutron diffraction. The radial component of the stress is near zero and left out for brevity. The two techniques agree qualitatively, but the stresses measured with neutron diffraction are consistently lower in magnitude than those determined by the contour method.

Taken in general, the residual stress profile is largely typical of an autogenous circumferential weld [35]. The differential heating during welding causes localized plasticity which results in a macroscopic residual stress field. Localized hot spots at and near the weld attempt to contract on cooling but are constrained by cold, rigid metal in

the surroundings, resulting in the typical tensile hoop stress near the weld and balancing compression in the far-field observed here and in many other published works.

The peak stresses are quite large and occur subsurface. The maximum tensile hoop stress determined by the contour method is roughly 300 MPa near the OD surface where neutrons cannot accurately probe. Tensile tests were performed on several samples taken from the cylinders. The results varied, presumably because of the large grain size, but showed yield stresses of about 200-250 MPa with strain hardening to over 400 MPa. The peak hoop stress exceeds the initial yield strength because of the multi-axial nature of the stress and the strain hardening of the material. Individual residual stress components exceeding nominal yield strength have been observed routinely in tensile stress regions near welds [36].

The detailed shape of the residual stress profile in the welded uranium cylinders, in particular the hoop component, closely matches the microstructural upset associated with the welding. The hoop stress shows a deep, narrow tensile maximum associated with the first pass of the focused electron beam. Because the weld does not penetrate fully, significantly less heat is deposited near the ID, lessening the severity of the hoop residual stress in this region. The second pass, with the electron beam de-focused, deposits heat predominantly near the outer surface causing the broad, shallow component of the observed residual stress field near the surface. Indeed, the localized heating near the outer surface at the weld drives the hoop component of the stress very near or into compression at the ID.

The axial stress profile is also related to the gradient of heat deposition through the thickness of the material during welding and the inability of tensile stresses to be

supported across the un-joined portion of the joint. The outer half of the cylinder near the weld reaches higher temperatures than the inner half and, thus, tries to contract more. Again, the constraint of the cooler metal results in the tensile axial stress at the OD and balancing compressive stress at the ID.

4.2 Critical Comparison of the Neutron Diffraction and Mechanical Relaxation Stress Measurements In the comparisons of the hoop component of the residual stress measured with diffraction and the contour method shown in both figures 9 and 10, the stresses measured with diffraction are consistently ~50 MPa below those measured with the contour method. As described in the introduction, the contour method has generally agreed well with neutron measurements, but sometimes not as well in materials or regions with texture or intergranular stresses [37, 38].

The consistent offset between the stresses measured with the two techniques suggests that the source of disagreement is the lack of absolute reference lattice parameter measurements with neutron diffraction. Given the stiffness of uranium, the ~50 MPa offset corresponds to an error ($\Delta d/d$) of roughly 0.25×10^{-4} in the selection of the reference. However, the fact that the stresses measured with neutron diffraction satisfy the boundary conditions and expectations (e.g. the radial and axial stresses are zero far from the weld) and overall force balance argues against an incorrect reference lattice parameter.

There are other sources of difference between the two measurement techniques that should be considered. The spatial averaging, in particular, that was necessitated by rotating the sample to increase the grain sampling could also cause the neutron stress measurement to be systematically low. The weld start and stop positions, which were not

identifiable on the weld, can destroy the cylindrical symmetry of the weld profile about the axis. Further, the joint fit may have varied around the weld, causing variations in the peak stress around the circumference. Regardless of the source, if the weld stresses vary circumferentially, then it is possible that the contour cut was done near a high point in the stress. The stresses determined from neutron diffraction, which averaged over the circumference would then appear low.

The two most common systematic errors associated with the contour method are unlikely to explain the difference in stress magnitudes measured by the two techniques. Because the measured stress magnitudes exceed the nominal yield strength, plasticity at the tip of the cut could have caused errors. Plasticity effects are difficult to predict because they depend on prior history, strain hardening and cyclic plasticity. Nonetheless, simulations of plasticity effects for the contour method indicate possible errors in the position and shape of the stress profile, but not significant increases in peak stress magnitudes[39, 40].

The contour method also assumes that the cut removes a constant width of material relative to the undeformed part. Because material ahead of the cut deforms as stresses are released, the cut width relative to the undeformed part evolves [41]. This error was reduced by securely clamping the part during cutting, but could still cause errors of 5% to 10% in magnitude and spatial misalignment of results by a small amount. These effects do not likely explain the differences between the stresses measured with contour and neutron diffraction techniques.

5. Conclusions

The residual stresses in an electron-beam welded cast uranium cylinder were measured by neutron diffraction and the contour method. Neutron strains were obtained from the three lattice parameters a , b and c of the orthorhombic crystal structure of uranium. Stresses were determined from the measured strains weighted by the observed spatially varying texture components. Large uranium grains necessitated rotating the cylinder continuously on its own axis to average around the circumference. For the contour method a novel two step process was used to relieve the bending moment stresses and minimize errors on the final cut. The analysis of the contour method data was modified from standard protocol in order to allow for a discontinuity in surface height across the un-joined portion of the partial penetration weld.

Given the complexity associated with orthorhombic uranium as well as the cylindrical geometry of the welded part and the large grained microstructure, the agreement between the two methods is reasonable. The results of the two techniques were very similar in trend but the neutron diffraction measured stresses were systematically ~ 50 MPa lower than those determined by the contour method near the weld, indicating a biasing error. Possible sources of this error in both techniques were discussed.

The observed stresses associated with the weld are conventional in form despite the anisotropic mechanical and thermal properties of crystalline uranium. High hoop stresses of roughly 300 MPa were found in the center of the weld near the OD with a strong through-thickness gradient. Also, a tensile axial stress (85 ± 25 MPa) was observed near the OD, again with a strong through-thickness gradient. The through-thickness gradients are related to the differential deposition of heat versus depth in the partial penetration weld.

6. Acknowledgements

The authors wish to thank Anne Kelly and Bob Forsyth for metallographic characterization, Tyler Wheeler and John Balog for contour method assistance, and Tim Beard and Isaac Cordova for depleted uranium machining. This work has benefited from the use of the Lujan Neutron Scattering Center at LANSCE, which is funded by the Office of Basic Energy Sciences (DOE). Los Alamos National Laboratory is operated by Los Alamos National Security LLC under DOE Contract DE-AC52-06NA25396.

References

- [1] Withers, P.J., Reports on Progress in Physics, 2007;70:2211.
- [2] Withers, P.J., Bhadeshia, H., Materials Science and Technology, 2001;17:355.
- [3] Carr, D.G., Ripley, M.I., Holden, T.M., Brown, D.W., Vogel, S.C., Acta Mat, 2004;52:4083.
- [4] Brown, D., Varma, R., Bourke, M., Ely, T., Holden, T., Spooner, S., ECRS 6: Proceedings of the 6th European Conference on Residual Stresses, 2002;404-4:741.
- [5] Hutchings, M.T., Withers, P.J., Holden, T.M., Lorentzen, T., Introduction to the Characterization of Residual Stress by Neutron Diffraction. Boca Raton: Taylor and Francis, 2005.
- [6] Brown, D.W., Bourke, M.A.M., Clausen, B., Korzekwa, D.R., Korzekwa, R.C., McCabe, R.J., Sisneros, T.A., Teter, D.F., Mat Sci Eng A, 2009;512:67.
- [7] Gittus, J.H., Metallurgy of the Rarer Metals : Uranium. London: Butterworths, 1963.
- [8] Sha, W., Wang, Y.H., Journal of Less Common Metals, 1989;146:179.
- [9] Eckelmeyer, K.H. Adv in Sur Treat Technol, vol. 4: Pergamon Press, 1987.
- [10] Salinas-Rodriguez, A., Root, J.H., Holden, T.M., Macewen, S.R., Ludtka, G.M. In: Shapiro SM, Moss SC, Jorgensen JD, editors. Materials Research Society, vol. 166. Pittsburgh, 1990. p.305.
- [11] Prask, H.J.A.C., C.S., J Nuc Matl, 1984;126:124.
- [12] Prime, M.B., Journal of Engineering Materials and Technology, 2001;123:162.
- [13] Kelleher, J., Prime, M.B., Buttle, D., Mummery, P.M., Webster, P.J., Shackleton, J., Withers, P.J., Journal of Neutron Research, 2003;11:187.
- [14] Hatamleh, O., International Journal of Fatigue, 2009;31:974.
- [15] DeWald, A.T., Hill, M.R., Journal of Strain Analysis for Engineering Design, 2009;44:13.
- [16] Thibault, D., Bocher, P., Thomas, M., Journal of Materials Processing Technology, 2009;209:2195.
- [17] Zhang, Y., Ganguly, S., Edwards, L., Fitzpatrick, M.E., Acta Mat, 2004;52:5225.
- [18] Prime, M.B., Sebring, R.J., Edwards, J.M., Hughes, D.J., Webster, P.J., Exp Mech, 2004;44:176.
- [19] Kartal, M., Turski, M., Johnson, G., Fitzpatrick, M.E., Gungor, S., Withers, P.J., Edwards, L., Mat Sci Forum, 2006;524/525:671.
- [20] Bouchard, P.J., International Journal of Pressure Vessels and Piping, 2007;85:152.
- [21] Kartal, M.E., Liljedahl, C.D.M., Gungor, S., Edwards, L., Fitzpatrick, M.E., Acta Mat, 2008;56:4417.
- [22] Turski, M., Edwards, L., International Journal of Pressure Vessels and Piping, 2009;86:126.
- [23] Smith, M.C., Smith, A.C., International Journal of Pressure Vessels and Piping, 2009;86:79.
- [24] Vamas-20, Technical Specification, ISO/TS 21432, 2005.
- [25] Bourke, M., Dunand, D., Ustundag, E., App Phys A, 2002;A74:S1707.
- [26] Oliver, E.C., private communications with E.C. Oliver, 2007.
- [27] Vondreele, R.B., Jorgensen, J.D., Windsor, C.G., J App Cryst, 1982;15:581.

- [28] Daymond, M.R., *J App Phys*, 2004;96:4263.
- [29] Kocks, U.F., Tome, C.N., Wenk, H.R., *Texture and Anisotropy*. Cambridge: Cambridge University Press, 1998.
- [30] Turner, P.A., Tome, C.N., *Acta Met*, 1994;42:4143.
- [31] Clausen, B., Tome, C.N., Brown, D.W., Agnew, S.R., *Acta Mat*, 2008;56:2456.
- [32] De Swardt, R.R., *Journal of Pressure Vessel Technology*, 2003;125:305.
- [33] Johnson, G. School of Materials, Ph.D.: University of Manchester, 2008.
- [34] Hill, M.R., Private Communication, 2003.
- [35] Dong, P., *Journal of Pressure Vessel Technology*, 2007;129:345.
- [36] Webster, G.A., Ezeilo, A.N., *International Journal of Fatigue*, 2001;23:S375.
- [37] Prime, M.B., Gnaupel-Herold, T., Baumann, J.A., Lederich, R.J., Bowden, D.M., Sebring, R.J., *Acta Mat*, 2006;54:4013.
- [38] Woo, W., Choo, H., Prime, M.B., Feng, Z., Clausen, B., *Acta Mat*, 2008;56:1701.
- [39] Shin, S.H., *Journal of Mechanical Science and Technology*, 2005;19:1885.
- [40] Dennis, R.J., Bray, D.P., Leggatt, N.A., Turski, M. . 2008 ASME Pressure Vessels and Piping Division Conference. Chicago, IL, USA: ASME, 2008. p.PVP2008.
- [41] Prime, M.B. SEM Conference & Exposition on Experimental & Applied Mechanics. Albuquerque, NM, USA: Society for Experimental Mechanics, Inc., 2009. p.and <http://www.lanl.gov/contour/>.

Table 1
Elastic constants and diffraction elastic constants for uranium (GPa).

	C_{11}	C_{22}	C_{33}	C_{12}	C_{13}	C_{23}	C_{44}	C_{55}	C_{66}
Single crystal stiffnesses	214.8	198.6	267.1	46.5	21.8	107.6	124.4	73.4	44.3
EPSC calculation	223.3	226.6	222.9	52.6	58.6	60.3	84.6	84.4	84.8
Bulk isotropic elastic constants [7]	220	220	220	58	58	58	81	81	81

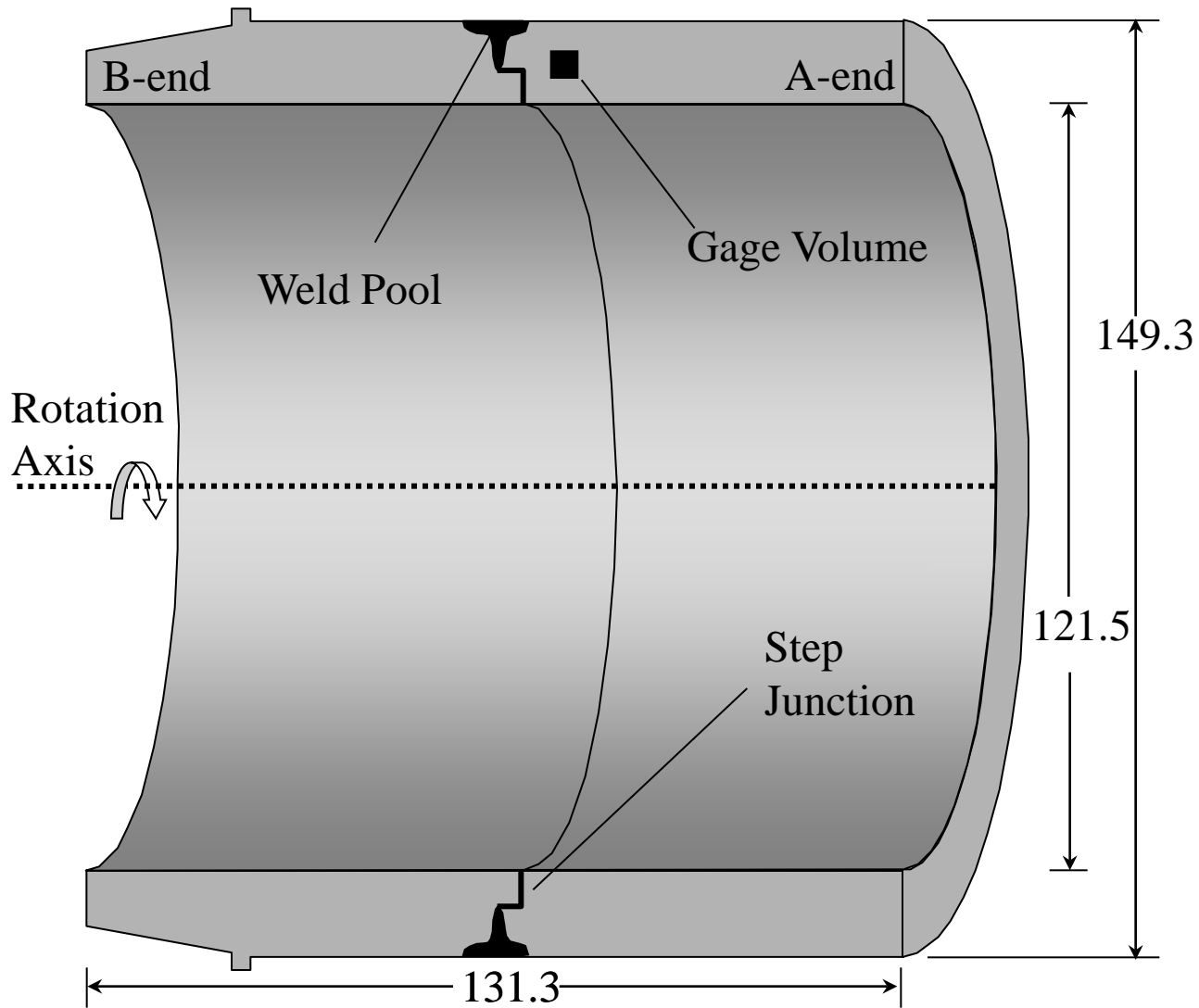


Figure 1. Schematic of the e^- beam welded uranium tube. Dimensions are approximately to scale. The black square represents the diagonal dimension of the irradiated gauge volume, that is ~ 4.5 mm.

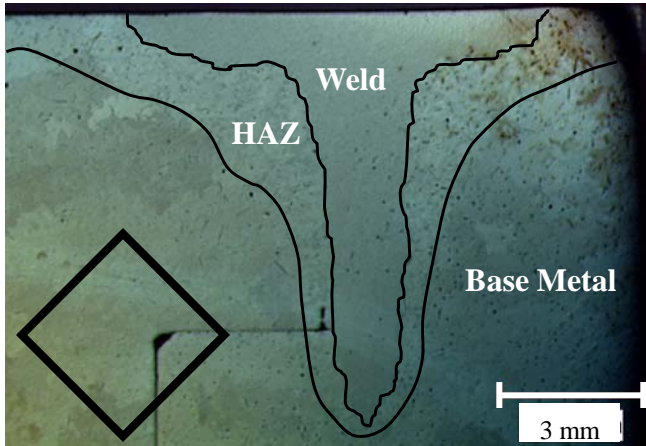


Figure 2. Macrograph of welded region. The diamond represents the irradiated gage volume when measuring the axial and radial components of the strain tensor. Weld pool and approximate HAZ are outlined for clarity.

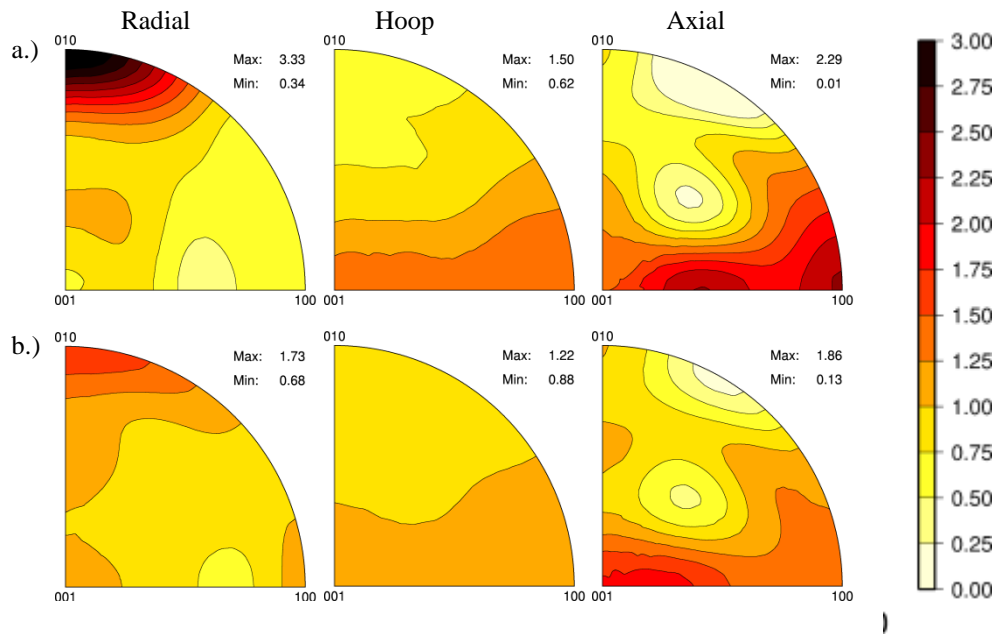


Figure 3. Inverse pole figures representing preferred orientations of crystallites along the indicated sample directions in the a.) base metal near the b end and b.) in the HAZ. The contours go from 0 MRD to 3 MRD at intervals of 0.25 MRD

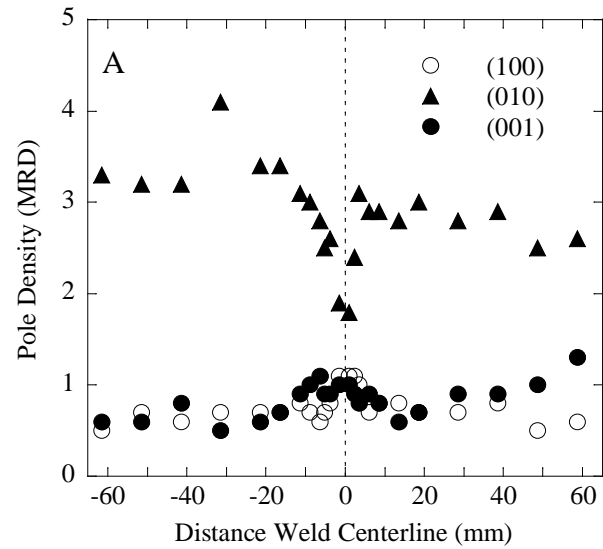


Figure 4. Pole density of the orthogonal crystal axes as a function of distance from the weld center. The “A-end” of the cylinder is on the negative side of the abscissa as indicated.

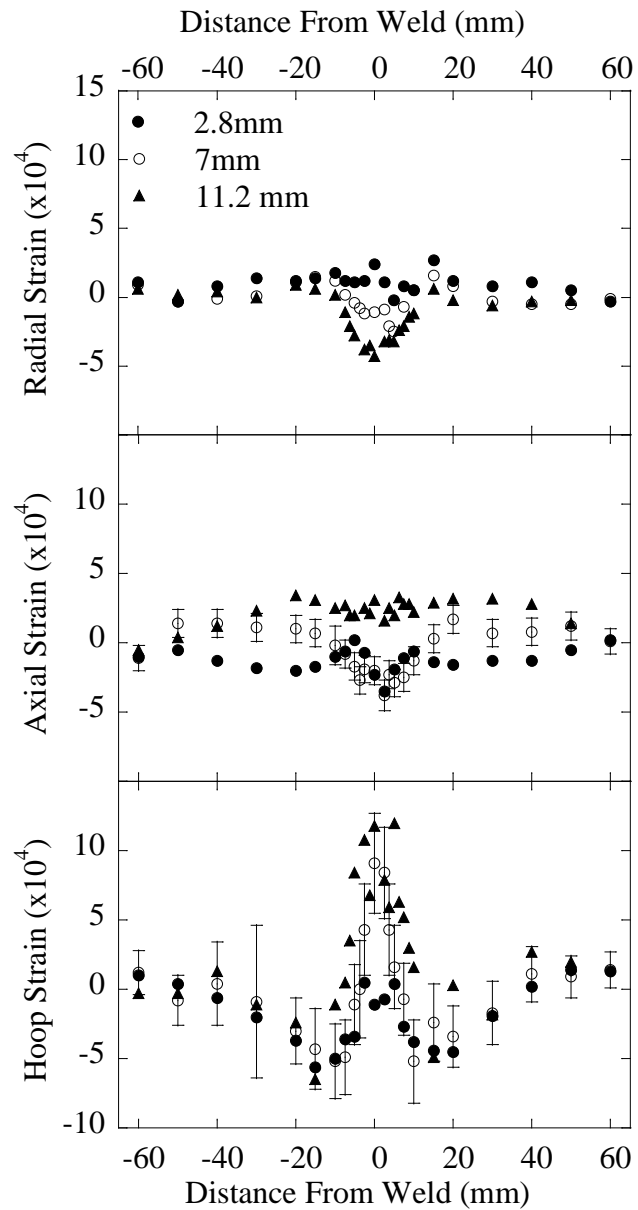


Figure 5. Radial, axial and hoop components of the residual strain as a function of distance from the weld center on three different through-thickness loci, 2.8 mm, 7.0 mm, and 11.2 mm from the ID.

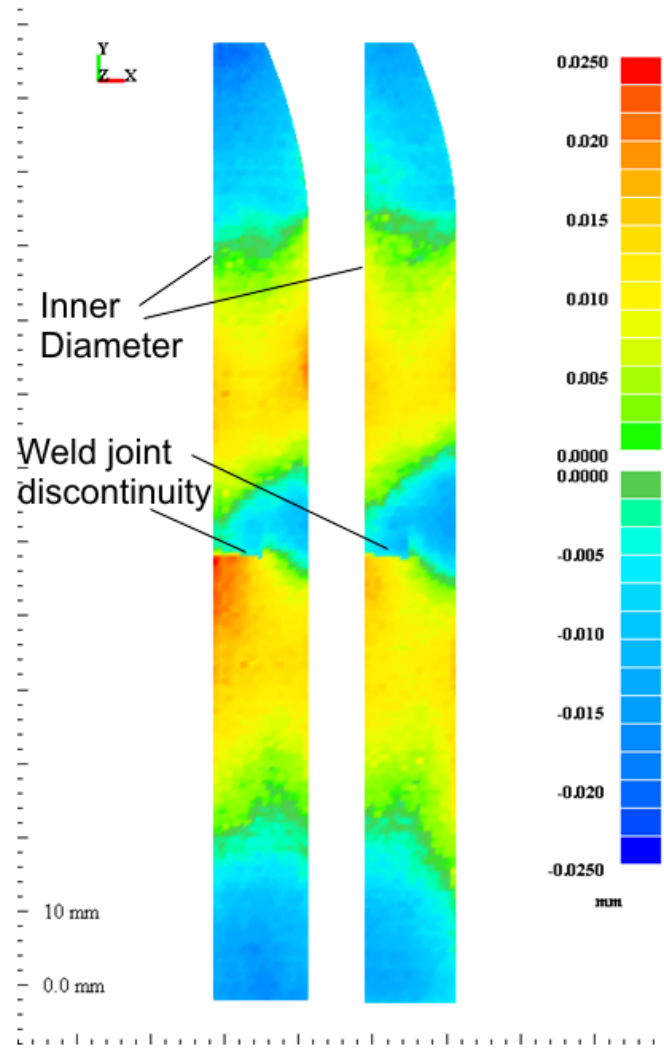


Figure 6. Surface height contours measured on the two opposing surfaces created by the cut show the expected low region near the weld and also a discontinuity at the unwelded portion of the joint, near the ID.

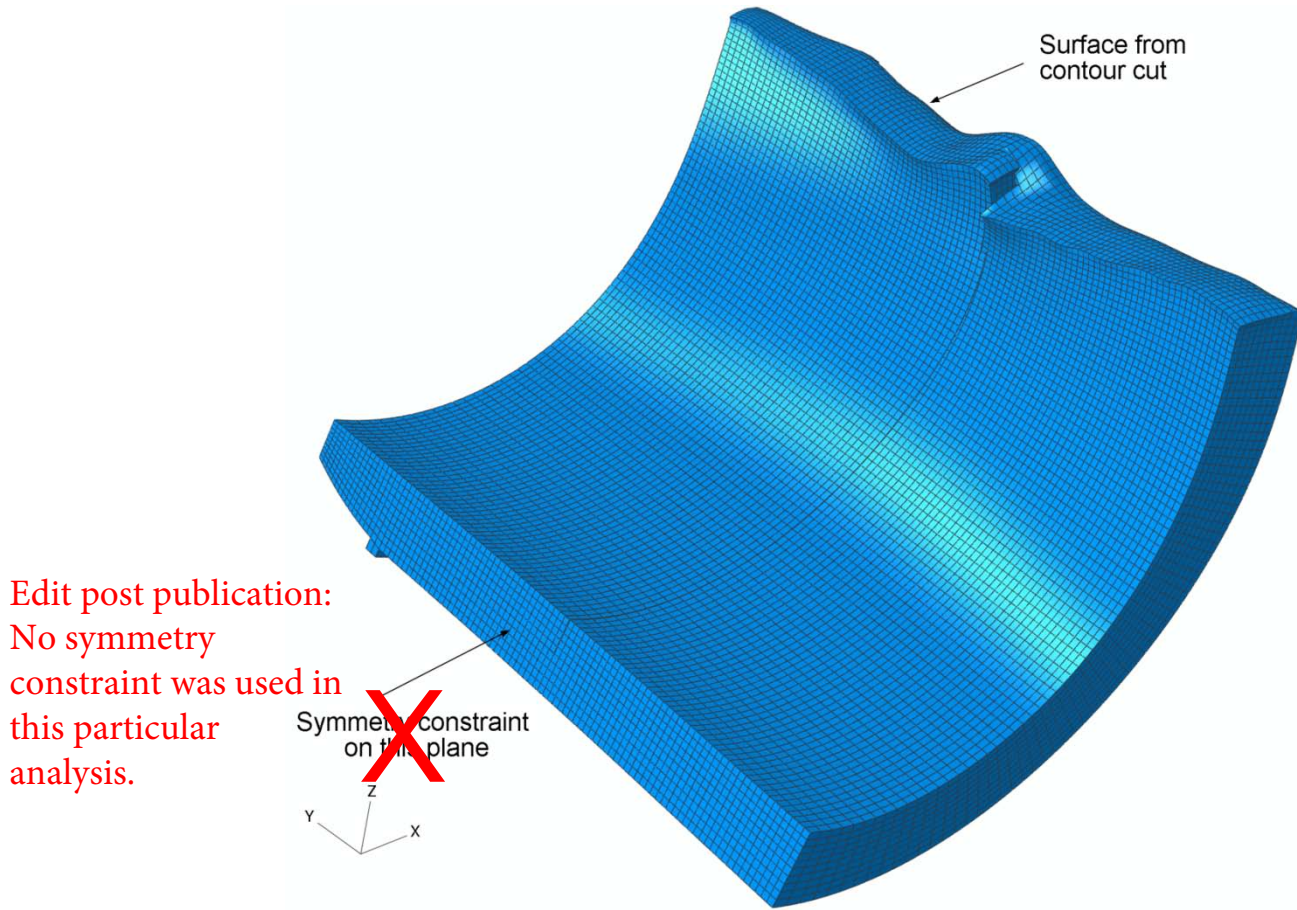


Figure 7. The finite element model of a section of the cylinder with the cut surface deformed into the opposite of the measured contour. Displacements magnified by a factor of 300.

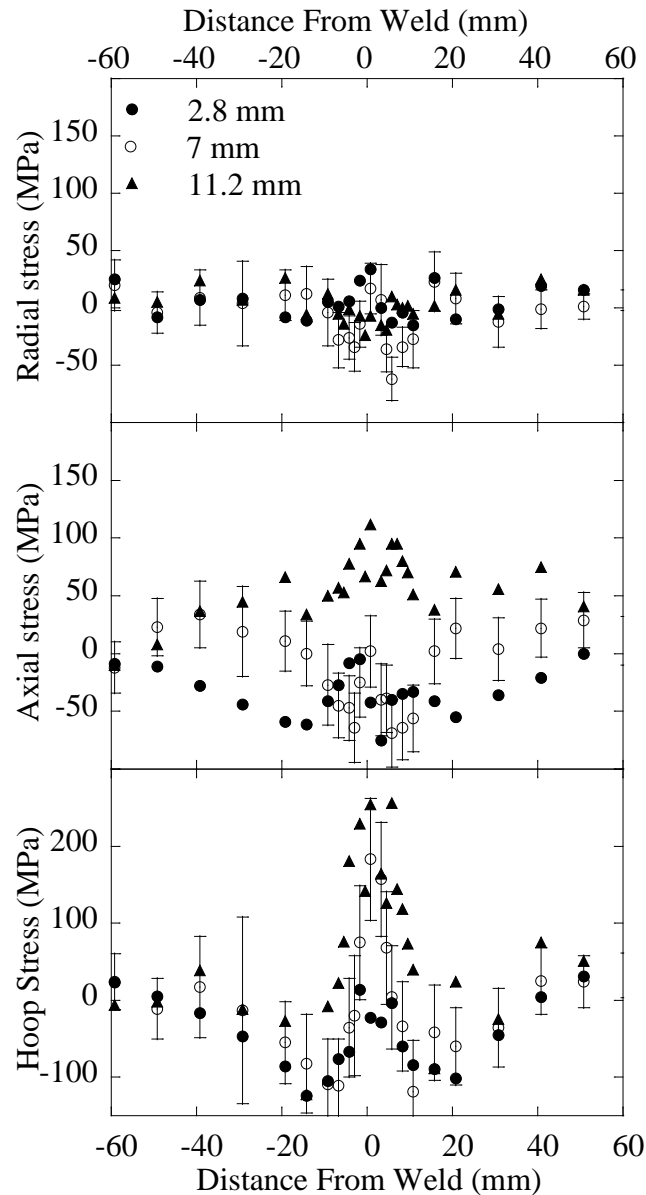


Figure 8. Radial, axial and hoop components of the residual stress measured by neutron diffraction as a function of distance from the weld center on three different through-thickness loci, 2.8 mm, 7.0 mm, and 11.2 mm from the ID. Note the different scale of the hoop stress relative to the radial and axial.

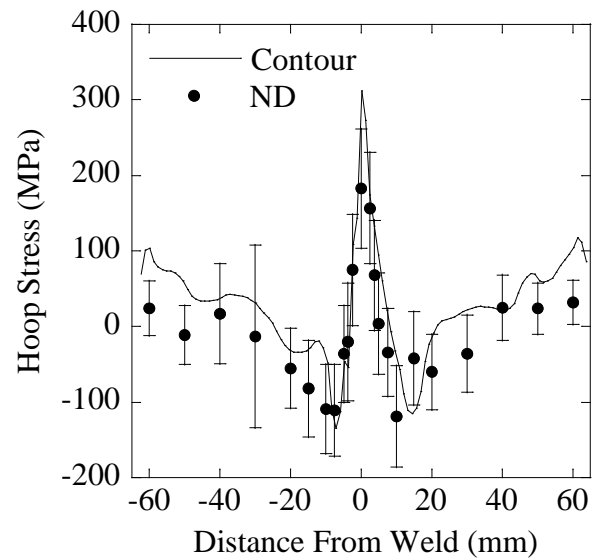


Figure 9. Hoop component of the residual stress as a function of distance from the weld at the center of the wall thickness. The line represents stresses determined by mechanical relaxation, the points by neutron diffraction.

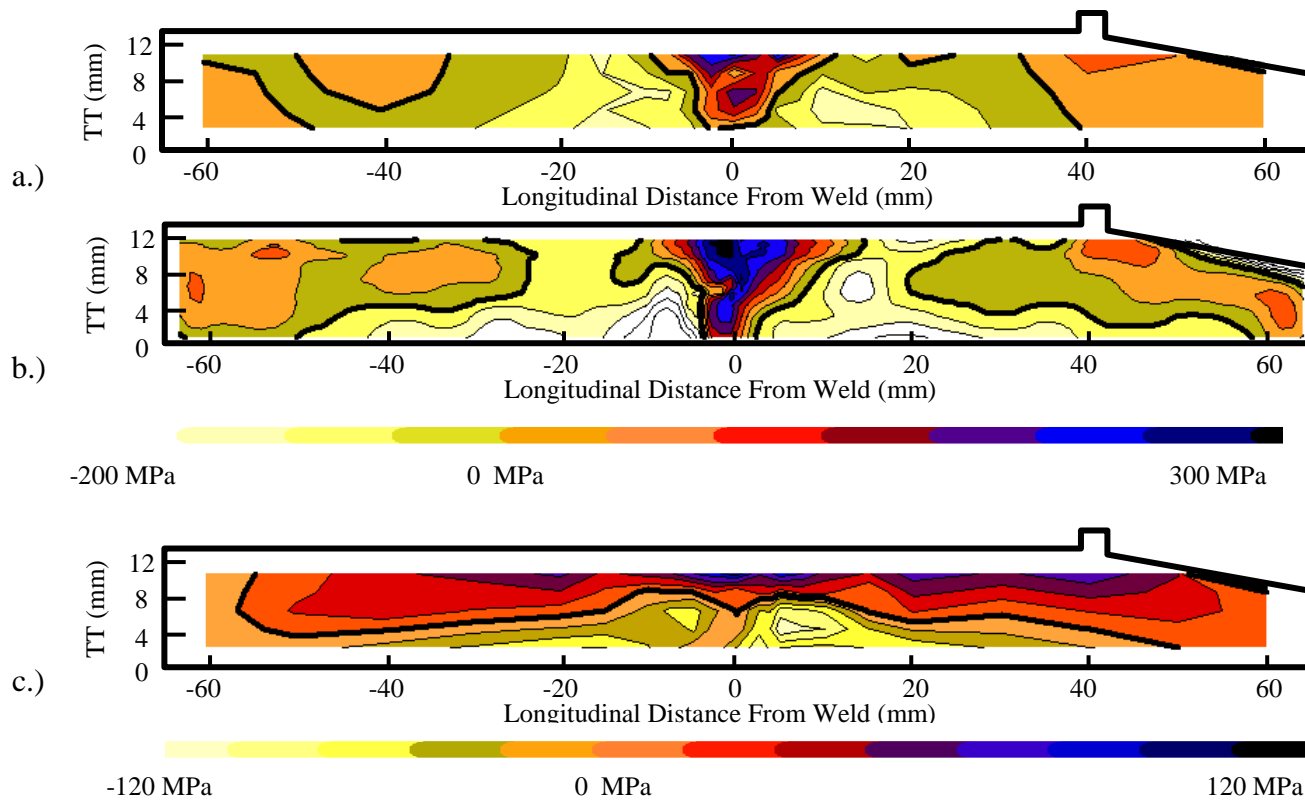


Figure 10. Contour plots of the hoop component of the residual stress measured with a.) neutron diffraction b.) the mechanical relaxation technique, and c) shows the axial component of the residual stress measured with neutron diffraction. Note the different scales for the different components of the stress. The hoop stress contours go from -200 MPa to 300 MPa with 25MPa intervals, while the axial stress contours go from -120 MPa to 120 MPa with 20 MPa contours. The bold contour represents 0 MPa in both cases.